

# UC Irvine

## Working Paper Series

### Title

Vehicle Point Cloud Reconstruction Framework for FHWA axle-based Classification using Roadside LiDAR Sensor

### Permalink

<https://escholarship.org/uc/item/2jf86859>

### Authors

Li, Yiqiao  
Tok, Andre  
Sun, Zhe  
[et al.](#)

### Publication Date

2021-08-02

1 **Vehicle Point Cloud Reconstruction Framework for FHWA axle-based Classification using**  
2 **Roadside LiDAR Sensor**

3  
4 **Yiqiao Li, Ph.D., Corresponding Author**

5 Assistant Project Scientist  
6 Department of Civil and Environmental Engineering  
7 Institute of Transportation Studies  
8 4000 Anteater Instruction and Research Building (AIRB)  
9 University of California, Irvine  
10 Irvine, CA 92697  
11 yiqiall@uci.edu

12  
13 **Andre Y.C. Tok, Ph.D.**  
14 Testbeds Manager and Assoc. Project Scientist  
15 Institute of Transportation Studies  
16 4000 Anteater Instruction and Research Building (AIRB)  
17 University of California, Irvine  
18 Irvine, CA 92697  
19 ytok@uci.edu

20  
21 **Zhe Sun, Ph.D.**  
22 Systems Manager  
23 Institute of Transportation Studies  
24 4000 Anteater Instruction and Research Building (AIRB)  
25 University of California, Irvine  
26 Irvine, CA 92697  
27 zhes@uci.edu

28  
29 **Stephen G. Ritchie, Ph.D.**  
30 Professor of Civil Engineering and  
31 Director, Institute of Transportation Studies  
32 4000 Anteater Instruction and Research Building (AIRB)  
33 University of California, Irvine  
34 Irvine, CA 92697  
35 sritchie@uci.edu

36  
37 **Koti Reddy Allu**  
38 Ph.D. Candidate  
39 Department of Civil and Environmental Engineering  
40 Institute of Transportation Studies  
41 4000 Anteater Instruction and Research Building (AIRB)  
42 University of California, Irvine  
43 Irvine, CA 92697  
44 kallu@uci.edu

45  
46  
47  
48 Word Count: 6,980 words + 1 table (250 words per table) = 7,230 words  
49 Submitted [Submission Date]

1 **ABSTRACT**

2 As Light Detection and Range (LiDAR) technologies rapidly advance, it is becoming increasingly viable  
3 as a solution to collect vehicle classification data. The main challenge of LiDAR compared with traditional  
4 image-based sensors in vehicle classification lies in its resolution, which limits the ability of LiDAR-based  
5 models to classify vehicles in detail from a single captured frame. This paper proposes a novel vehicle point  
6 cloud reconstruction framework with the consideration of the ground plane constraint and develops a  
7 bootstrap aggregating deep neural network (bagging DNN) model to classify the reconstructed vehicle point  
8 clouds based on the FHWA classification scheme. First, the FilterReg registration algorithm is used to  
9 estimate the transformation matrix between consecutive frames of each vehicle point cloud. Then, a  
10 multiway registration is conducted to fine-tune the estimated transformation matrices to rebuild the 3D  
11 model of each moving vehicle. Second, the key features are extracted from the reconstructed vehicle models  
12 and fed into a bagging DNN model to classify them based on the FHWA classification scheme. The initial  
13 field test shows that this reconstruction framework can correctly reconstructing vehicle objects with a  
14 tolerance of 3-5 consecutive missing frames. The classification model with the reconstruction framework  
15 outperforms the state-of-the-art LiDAR-based FHWA classification model in terms of both accuracy and  
16 robustness. The model has a 79 percent average correct classification rate (CCR). Remarkably, the proposed  
17 model can accurately distinguishing Classes 5, and 8 trucks, which have overlapping axle configurations  
18 with a 97 percent and an 84 percent CCR, respectively.

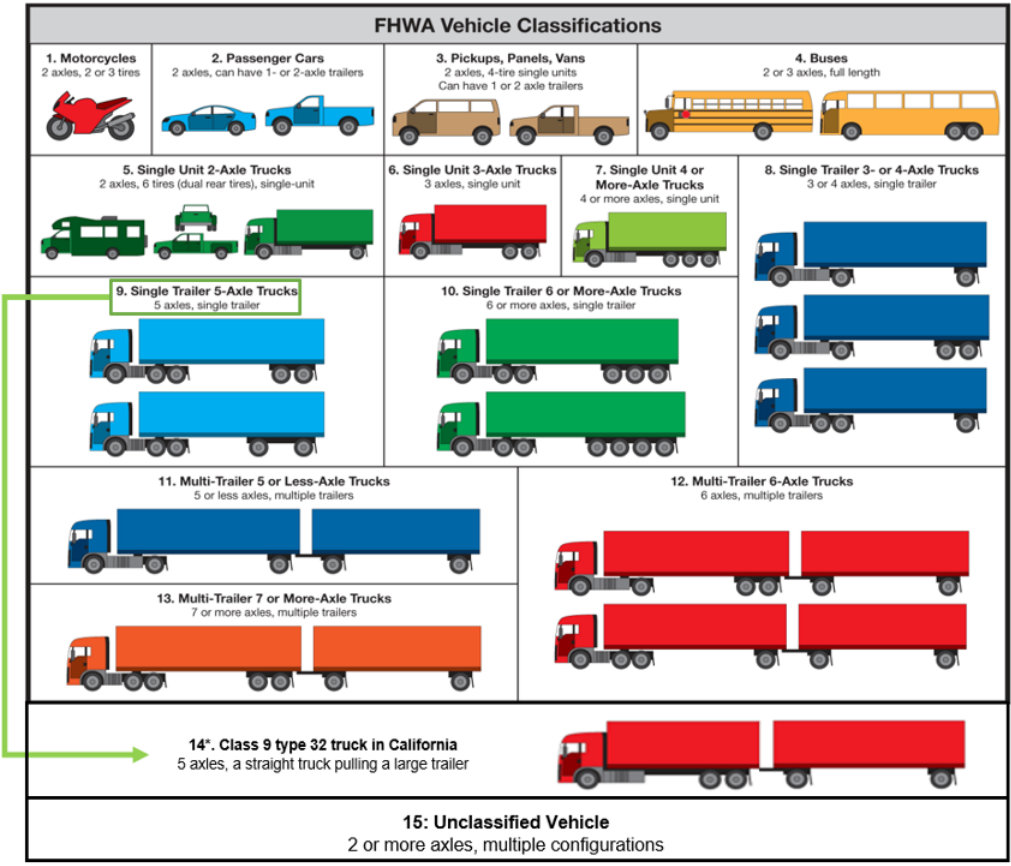
19

20 *Keywords:* LiDAR, Vehicle Point Cloud Reconstruction, Point Cloud Registration, FHWA Vehicle  
21 Classification, Bootstrap Aggregating Deep Neural Network.

22

1 **1. Introduction**

2 Truck classification data is an essential data source that is commonly used in various transportation  
 3 applications, such as pavement design (1), on-road emission estimation (2) and freight planning (3, 4). In  
 4 order to serve the needs of different transportation data users, the Federal Highway Administration (FHWA)  
 5 uses a standardized vehicle classification scheme that classifies vehicles according to their tire and axle  
 6 combinations while considering the general body configurations of vehicles (5). The State of California  
 7 used a slightly modified scheme (FHWA-CA) which splits Class 9 trucks – 5 axle single trailer trucks –  
 8 into two distinct categories, as presented in Figure 1.



Note: \* FHWA-CA distinguishes 5-axle straight trucks pulling full trailers (Class 9 Type 32) from other Class 9 trucks in the 13-category FHWA Scheme to form a standalone Class 14 category.

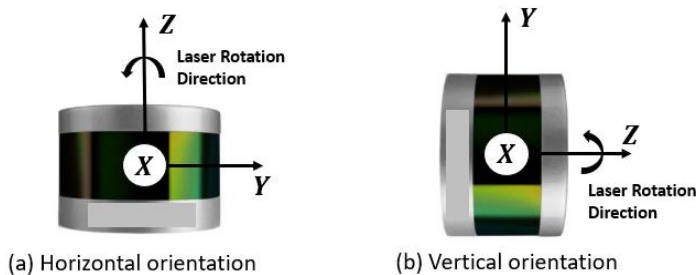
9  
 10 Figure 1 FHWA-CA Classification Scheme Definitions (6)

11 Axle classification data is generally collected at vehicle classification sites equipped with Weigh-In-Motion  
 12 (WIM) systems (6) or piezoelectric sensors (7). In addition, researchers also investigated using sensors such  
 13 as embedded strain gauges (8) and the in-pavement wireless sensor system including accelerometer sensors  
 14 and magnetometer sensors (9, 10) to obtain FHWA classification data. However, the spatial coverage of  
 15 these classification sites is typically limited because of their high installation and maintenance costs. On  
 16 the other hand, inductive loop sensors are cheaper to install and maintain and are ubiquitous across the U.S  
 17 highway network for traffic monitoring operations. As a consequence, researchers also explored the use of  
 18 inductive vehicle signature data retrieved from the advanced loop detector to classify vehicles based on the  
 19 FHWA classification scheme (11, 12). Unfortunately, the coverage of the inductive loop sensors remains  
 20 limited along rural highway corridors that also contribute significantly to the economy. However, the  
 21 installation of pavement intrusive sensors requires inevitable pavement cuttings and lane closures which

1 are cost-inefficient. Hence, it may be impractical to implement pavement intrusive sensors extensively  
2 along rural highway corridors. Therefore, researchers have been starting to investigate using non-intrusive  
3 solutions, such as video cameras (13) and the Light Detection and Ranging (LiDAR) sensor, to obtain  
4 FHWA vehicle classification data.

5 LiDAR technology was initially researched for vehicle classification applications in the early 2000s when  
6 scanning laser sensors were available for roadside traffic surveillance. Such sensors scan the cross-section  
7 of the roadway by taking several range measurements for the vehicle passing through the scanning area  
8 (14–16). These studies adopted an overhead sensor mounting configuration to capture detailed information  
9 on each passing vehicle. However, the overhead mounting is subjected to the infrastructure constraint. Lee  
10 and Coifman mounted two vertically oriented laser scanners on a probe vehicle parked at the roadside to  
11 capture vehicles traversing the LiDAR detection zone (LDZ) (17). This speed-trap-like configuration  
12 allowed them to capture vehicle length-related features and classify vehicles according to a length-based  
13 scheme (17). However, the vertically-oriented laser scanners provide a very narrow field of view, meaning  
14 that one occluded frame may result in a significant information loss and negatively affect the performance  
15 of their classification model. Asborno et al. explored using a cost-efficient and practical single-beam  
16 LiDAR with a roadside setup to get truck body type information (18). They grouped the raw distance  
17 measurements from the LiDAR sensor over time to build vehicle signatures and adopted a Bayesian  
18 combined predictor to classify trucks based on their aggregated body type classes. However, the low-cost  
19 single-beam LiDAR sensor cannot provide detailed vehicle profiles, which reduces the classification  
20 accuracy and the diversity of vehicle types that can be classified. For instance, classes from the FHWA  
21 classification scheme are defined primarily on vehicle axle configurations which are not well-defined in the  
22 vehicle point cloud profiles extracted from the aforementioned sensors.

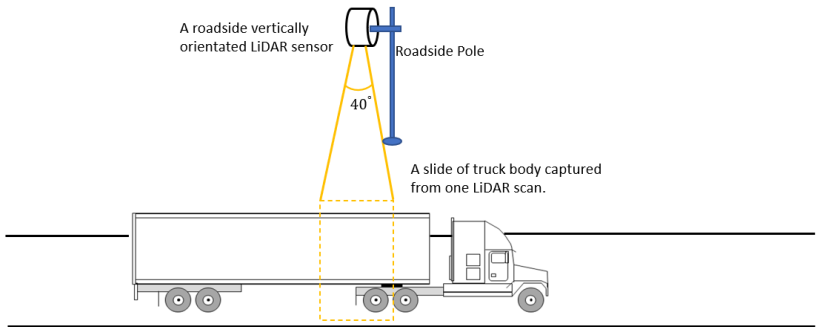
23 In recent years, multi-array rotating LiDAR sensors have become popular due to the sensing needs of  
24 autonomous vehicles. This type of sensor was designed to install on the top of the vehicles to perceive the  
25 ambient environment. Nezat et al. (19) made the first attempt to use such sensors to collect vehicle  
26 classification data. They mounted the LiDAR in a vertical orientation on a roadside pole. Figure 2 illustrates  
27 the LiDAR orientations that have been used throughout the literature.



28

29 Figure 2 Illustration of LiDAR Orientation (20)

30 When a truck enters the LiDAR Detection Zone (LDZ), each scan of the vertically orientated sensor  
31 captures a 3D profile of one side of the truck body within the scanning area. The vertical orientation of the  
32 sensor limits the detection zone to a 40-degree horizontal view as shown in Figure 3. All point cloud frames  
33 associated with the target vehicle were subsequently stitched together to generate the full profile of the  
34 truck (19) (21) and subsequently classify them.



1

2 Figure 3 Truck point clouds collection from vertically oriented LiDAR

3 The vertical orientation of the multi-array rotating 3D LiDAR is able to capture a dense representation of  
 4 each vehicle but significantly compromise the robustness of the classification framework. Wu et al utilized  
 5 a horizontally oriented LiDAR sensor, which provides a 360-degree field-of-view of roadways (22). When  
 6 a vehicle fully enters the LDZ, a single scan can cover the entire profile of the vehicle. Essential features  
 7 are extracted from the point cloud from a single scan of each vehicle and classified according to the FHWA  
 8 scheme. Unfortunately, the sparse point cloud representation retrieved from the horizontally oriented  
 9 LiDAR provides insufficient information for detailed truck classification, which likely limited the  
 10 performance of their classification model.

11 This study investigated the design of a novel vehicle point cloud reconstruction framework to match  
 12 consecutive frames of each vehicle by leveraging existing registration algorithms (23, 24) and adding a  
 13 ground plane constraint to accommodate transportation applications. The reconstructed vehicle point clouds  
 14 provide a dense representation of each vehicle object and retain the critical features that can be used to  
 15 accurately classify them according to the FHWA-CA scheme.

16 The rest of the paper is organized as follows. Section two describes the technical aspects of the data  
 17 collection setup and point cloud data preprocessing procedure: including background subtraction and data  
 18 association. Section three reviews commonly used point cloud registration algorithms and illustrates the  
 19 vehicle point cloud reconstruction framework adopted in this study. Section four describes the feature  
 20 extraction steps and the development of the vehicle classification model using a deep ensembled neural  
 21 network. Section five presents the results of the vehicle classification model and compares the proposed  
 22 model with the state-of-art LiDAR-based FHWA classification model. This paper concludes with a  
 23 discussion on the model results and potential future research pathways.

24

25

26

27 **2. Data Collection, Description, and Preprocessing**

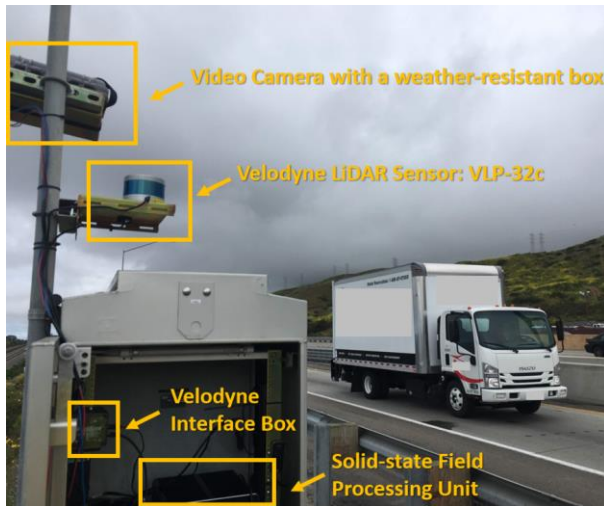
28 This section contains two parts: an overview of the data collection setup followed by a description of the  
 29 preprocessing of the LiDAR data from the raw point cloud to the attaining of each vehicle object group.

30 **2.1 Data Collection**

31 The data used in this study was collected from the entrance ramp into the San Onofre Truck Scale from the  
 32 southbound of the I-5 freeway. This is a major truck corridor between Orange and San Diego Counties in

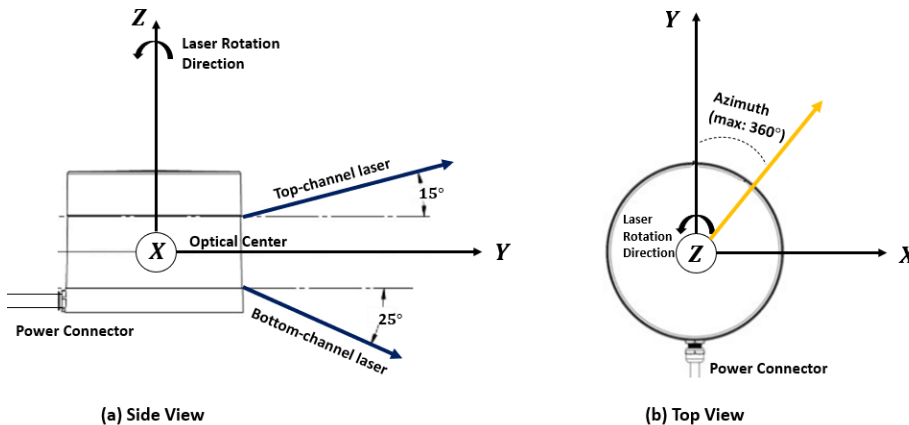
1 California, which is an ideal location for capturing a wide variety of truck types across the FHWA-CA  
2 scheme, except Classes 4 and 13 were not observed during the data collection period. The data was collected  
3 between July 18<sup>th</sup> and August 5<sup>th</sup>, 2019, including both free flow and congestion conditions with vehicle  
4 speeds ranging from 0 to 50 mph.

5 The San Onofre truck detection site was equipped with a video camera to establish data groundtruth and a  
6 Velodyne VLP-32c LiDAR unit for data collection. Both the video camera and the LiDAR unit were  
7 synchronized and connected to a solid-state field processing unit. The data collection setup is shown in  
8 Figure 4.



10 Figure 4 Data Collection Setup

11 The LiDAR sensor was horizontally placed on a flat platform which was elevated approximately 2 meters  
12 above the ground. The optical center of the LiDAR sensor was parallel to the ground plane. The illustration  
13 of the LiDAR sensing unit is shown in Figure 5.

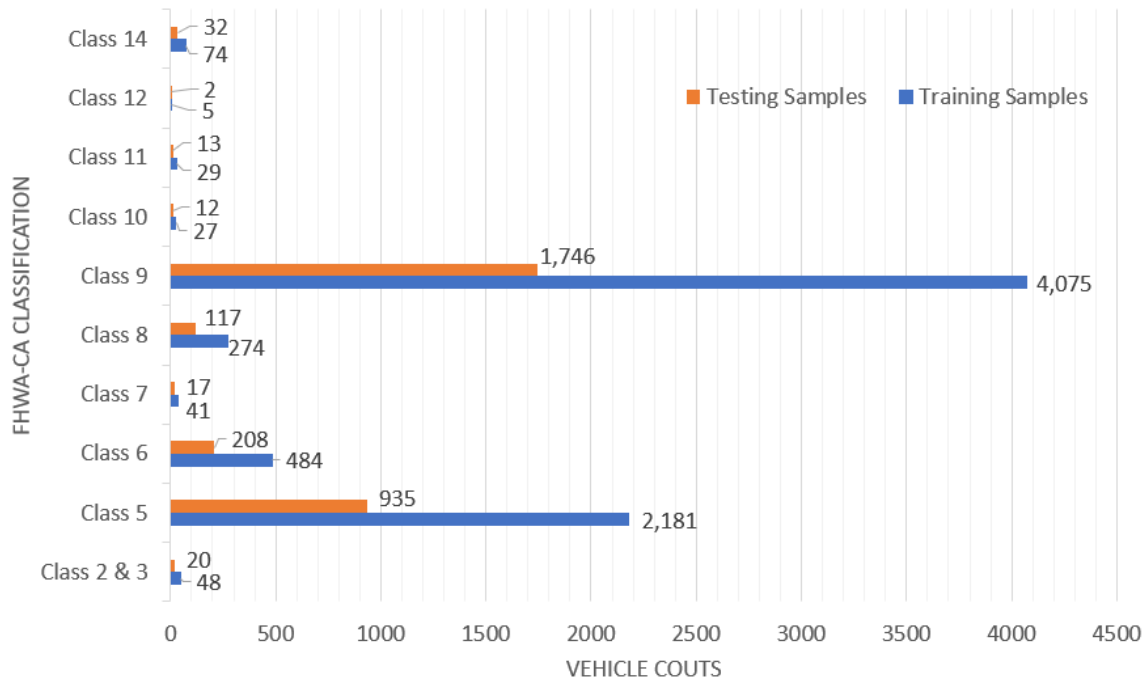


15 Figure 5 The Illustration of the LiDAR Sensing Unit

## 16 2.2 Data Description

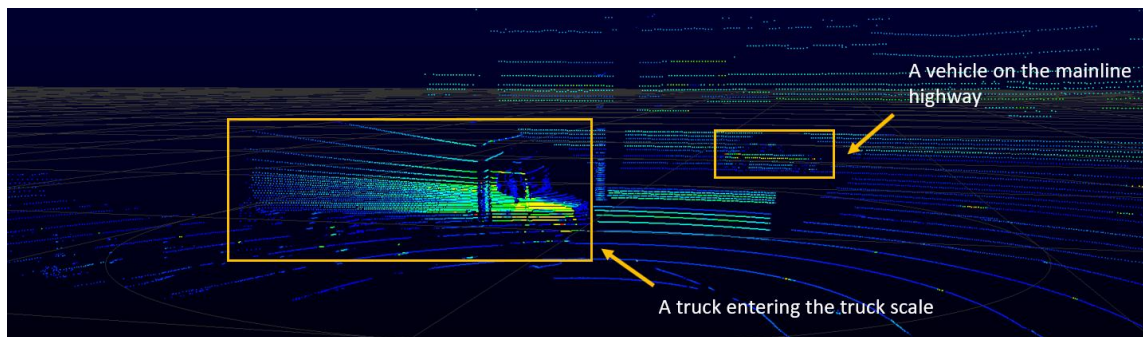
17 The system collected and processed data from 10,338 vehicles. All of them have been labeled through  
18 visual verification from the still images captured by the video camera. The labeled dataset was partitioned

1 into a 70-30 split for training and testing, respectively, using stratified sampling by FHWA classes. The  
 2 labeled FHWA vehicle class distribution is presented in Figure 6.



3  
 4 Figure 6 The FHWA-CA Class distribution of overall model development dataset

5 As shown in Figure 6, both Classes 4 and 13 vehicles were not observed in this dataset. Classes 2 and 3  
 6 were combined in a single class since both represent passenger vehicles with a small sample size when they  
 7 were used as standalone classes. The dataset will be further enriched in future work.



8  
 9 Figure 7 A Raw LiDAR Frame

10  
 11 2.3 Data Preprocessing  
 12 2.3.1 Background Substitutions and Object Detection

13 As illustrated in Figure 7, each raw LiDAR scan contains both the static roadway environment as  
 14 well as the vehicle objects of interest. Prior to the modeling process, points belonging to each  
 15 vehicle point cloud need to be segmented from the background environment – which are irrelevant



1 to the task of vehicle classification – and grouped into vehicle objects. This research adopted the  
 2 background subtraction and object detection method proposed in (25). The background subtraction  
 3 method first divided the conical surface generated by the LiDAR sensor into annular sector-shaped  
 4 cells. Then, the foreground vehicle point clouds and the background environment are split  
 5 according to the spatial occupancy of each cell. Finally, the segmented vehicle point cloud was  
 6 grouped and identified as a vehicle based on their points’ proximity using Density-based spatial  
 7 clustering of applications with noise (DBSCAN) clustering algorithm (26).

### 8 2.3.2 Data Association

9 This research utilized the Simple Online and Realtime Tracking (SORT) algorithm to associate a vehicle  
 10 point cloud from each LiDAR frame to its corresponding vehicle object efficiently (27). First, each vehicle  
 11 point cloud was represented by the centroid of the minimum oriented 2D bounding box which was obtained  
 12 from its ground projection. Next, the inter-frame displacements of each vehicle point cloud were estimated  
 13 using a linear constant velocity model - Kalman Filter (28). Finally, the vehicle point clouds were optimally  
 14 assigned to their corresponding vehicle object group using the Hungarian algorithm (29). An advantage of  
 15 the SORT framework is its ability to handle short-term occlusion caused by passing objects, although this  
 16 capability was not tested in our study (27).

17

## 18 3. Truck Point Cloud Registration Framework

### 19 3.1 Point Cloud Registration

#### 20 3.1.1 Introduction to Point-Set Registration

21 Point-set registration is an essential process widely used in the field of robotics and computer vision domain  
 22 to rebuild the model of a 3D object from the point cloud fragments obtained by moving robots equipped  
 23 with LiDAR sensors. It involves the estimation of the spatial transformation (e.g. translation, rotation, and  
 24 scaling) that aligns two sets of points associated with the same object from a sensor that captures them from  
 25 different views. For two given corresponding point sets  $P = \{\mathbf{p}_1, \mathbf{p}_2, \mathbf{p}_3, \dots, \mathbf{p}_m\}$  and  $Q =$   
 26  $\{\mathbf{q}_1, \mathbf{q}_2, \mathbf{q}_3, \dots, \mathbf{q}_n\}$  in  $\mathbb{R}^d$  ( $d$  represents the dimensions of each point, where  $d = 3$  in this study), the goal of  
 27 registration is to search for an optimal rigid transformation matrix  $\mathbf{T}_{PQ}$  composed of a rotation matrix  
 28  $\mathbf{R}(\theta_x, \theta_y, \theta_z)$  and a translation vector  $\mathbf{t}(t_x, t_y, t_z)$  to match point set  $P$  with point set  $Q$ .  $\theta_x, \theta_y, \theta_z$  represent  
 29 the counter-clockwise rotation angle of the point set about the  $x, y, z$  axis, respectively.  $t_x, t_y, t_z$  denote the  
 30 translation of the point cloud along the corresponding axis. In a homogeneous coordinate, a transformation  
 31 matrix  $\mathbf{T}_{PQ}$  that is used to align point set  $P$  and  $Q$  can be expressed as:

$$32 \quad \mathbf{T}_{PQ} = \mathbf{T}_{PQ}(\theta_x, \theta_y, \theta_z, t_x, t_y, t_z) = \begin{bmatrix} \mathbf{R} & \mathbf{t} \\ \mathbf{0} & 1 \end{bmatrix} \quad (1)$$

33 The 3D rotation about  $x, y, z$  axis ( $\mathbf{R}_x, \mathbf{R}_y, \mathbf{R}_z$ ) and translation matrix  $\mathbf{T}$  is shown below:

$$34 \quad \mathbf{R}_x = \begin{bmatrix} 1 & 0 & 0 & 0 \\ 0 & \cos\theta_x & -\sin\theta_x & 0 \\ 0 & \sin\theta_x & \cos\theta_x & 0 \\ 0 & 0 & 0 & 1 \end{bmatrix}, \mathbf{R}_y = \begin{bmatrix} \cos\theta_y & 0 & \sin\theta_y & 0 \\ 0 & 1 & 0 & 0 \\ -\sin\theta_y & 0 & \cos\theta_y & 0 \\ 0 & 0 & 0 & 1 \end{bmatrix}, \mathbf{R}_z = \begin{bmatrix} \cos\theta_z & -\sin\theta_z & 0 & 0 \\ \sin\theta_z & \cos\theta_z & 0 & 0 \\ 0 & 0 & 1 & 0 \\ 0 & 0 & 0 & 1 \end{bmatrix}, \mathbf{T} = \begin{bmatrix} 1 & 0 & 0 & t_x \\ 0 & 1 & 0 & t_y \\ 0 & 0 & 1 & t_z \\ 0 & 0 & 0 & 1 \end{bmatrix} \quad (2)$$

35 The most classic method used for solving point set registration problems is called the iterative closest point  
 36 (ICP) algorithm (30). The ICP algorithm starts with the initial transformation matrix  $\mathbf{T}_0 = (\mathbf{R}_0, \mathbf{t}_0)$  and

1 then selects a set of  $k$  corresponding points pairs  $(\mathbf{p}_i, \mathbf{q}_i)$  between point sets  $P$  and  $Q$ . The distance between  
 2  $P$  and  $Q$  can be written as:

$$3 \quad \text{dist}(\mathbf{T}_{PQ}(P), Q) \quad (3)$$

4  $\mathbf{T}_{PQ}(P)$  represents rotating and translating  $P$  with a transformation matrix  $\mathbf{T}_{PQ}$ .  $\text{dist}()$  denotes the distance  
 5 between point sets. There are two common ways found in the literature to define the distance between point  
 6 sets: Point-to-Point (30) and Point-to-Plane distance (31).

### 7 1. Point-to-Point Distance Evaluation (30)

8 Assuming  $N$  corresponding point pairs  $(\mathbf{p}_i, \mathbf{q}_i)$ ,  $i = 1 \dots N$ , the registration problem using point-to-point  
 9 distance measurement can be formulated as:

$$10 \quad \text{argmin}_{\mathbf{T}_{PQ}} \frac{1}{N} \sum_{i=1}^N \|\mathbf{T}_{PQ}\mathbf{p}_i - \mathbf{q}_i\|^2, \quad \text{s.t. } R^T R = I \quad (4)$$

11

### 12 2. Point-to-Plane Distance Evaluation (31)

13 When Point-to-Plane distances are used as the error metric, the objective function can be formulated as the  
 14 sum of the square error between  $\mathbf{p}_i$  and the tangent plane at  $\mathbf{q}_i$ . The norm of the tangent plane at  $\mathbf{q}_i$  is  
 15 denoted as  $\mathbf{nor}_i$ . The objective function is shown below:

$$16 \quad \text{argmin}_{\mathbf{T}_{PQ}} \frac{1}{N} \sum_{i=1}^N \|(\mathbf{T}_{PQ}\mathbf{p}_i - \mathbf{q}_i) \cdot \mathbf{nor}_i\|^2, \quad \text{s.t. } R^T R = I \quad (5)$$

17 The next step of the ICP algorithm is to iteratively find the optimal  $\mathbf{T}_{PQ}$  which minimize the distance  
 18 between  $P$  and  $Q$ . Due to the simplicity of the original algorithm, hundreds of ICP-based variants have been  
 19 proposed over the past two decades where a comprehensive review of ICP-based methods has been  
 20 documented in (32).

### 21 3.1.2 Probabilistic Point-set Registration

22 However, the performance of ICP-based approaches suffers from the noisiness, outliers, and occlusions of  
 23 point sets which commonly occur in a real-world dataset from an outdoor environment (33)(34). Many  
 24 researchers have investigated probabilistic approaches in an attempt to improve the robustness of point-set  
 25 registration. The most popular probabilistic-based registration algorithm is called Coherent Point Drift  
 26 (CPD) proposed by Myronenko and Song (34), which treated registration as a probability density estimation  
 27 problem. Instead of using the closest distance to define the corresponding point pairs, CPD assigns a  
 28 probability value to the correspondence according to the proximity between points from two point sets.  
 29 Several studies have investigated new probabilistic approaches to further enhance the robustness of the  
 30 registration algorithms (35–37). Unfortunately, such approaches typically gain robustness at the expense  
 31 of computation efficiency. Gao and Tedrake (23) developed a computationally efficient probabilistic-based  
 32 registration model - FilterReg - which adopted the Gaussian filtering methods to enhance the model  
 33 efficiency as well as preserve the robustness and accuracy of the registration process. FilterReg has been  
 34 proven to be computationally faster than the modern ICP variants (23). Therefore, this research adopted the  
 35 FilterReg algorithm to estimate transformation matrices between consecutive frames.

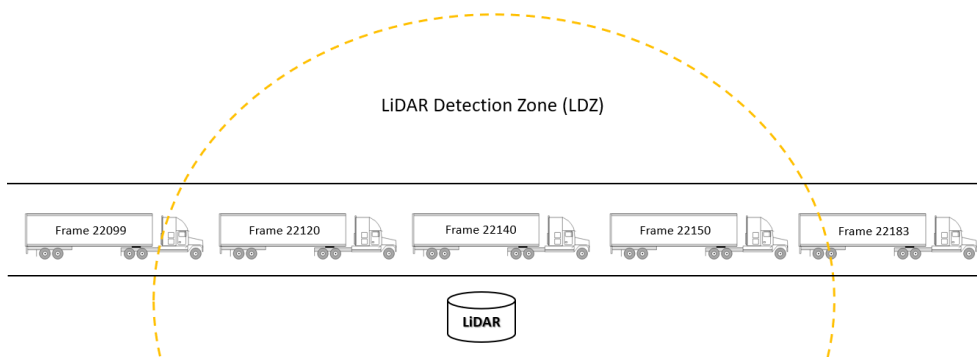
1 3.2 Vehicle Point Cloud Registration Framework

2 Previous research on point-set registration has mainly focused on aligning point-sets obtained from mobile  
3 sensors, where the LiDAR unit is equipped on the top of a moving robot (32) which allows the sensor to  
4 actively capture the object point clouds. As a consequence, point cloud density associated with the same  
5 object is relatively uniform across LiDAR frames. However, LiDAR sensors are generally mounted in side-  
6 fire orientation by the roadside for traffic surveillance research applications (17–19, 21). As a vehicle  
7 traverses the LDZ, the density of its point cloud will gradually increase and then decrease along with its  
8 proximity to the sensor. Therefore, this study modified the existing point-set registration framework to  
9 better adapt the data characteristics of vehicle point clouds collected from roadside LiDAR sensors and  
10 then to provide promising vehicle point cloud registration results to support the needs of FHWA axle-based  
11 vehicle classification.

12

13 3.2.1 Eliminate Redundant Frames

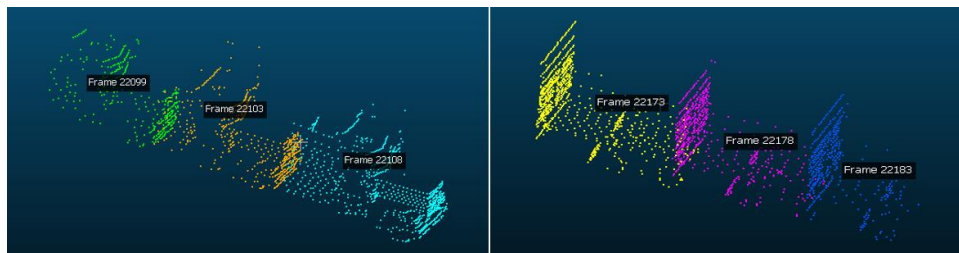
14 When a truck is entering or leaving the LDZ (Figure 8), its distance from the LiDAR sensing unit results in  
15 a sparse point cloud (Figure 9).



16

17 Figure 8 Samples of Truck Frames

18 Those frames generally depict the driving unit and the rear edge of the truck as shown in Figure 9.

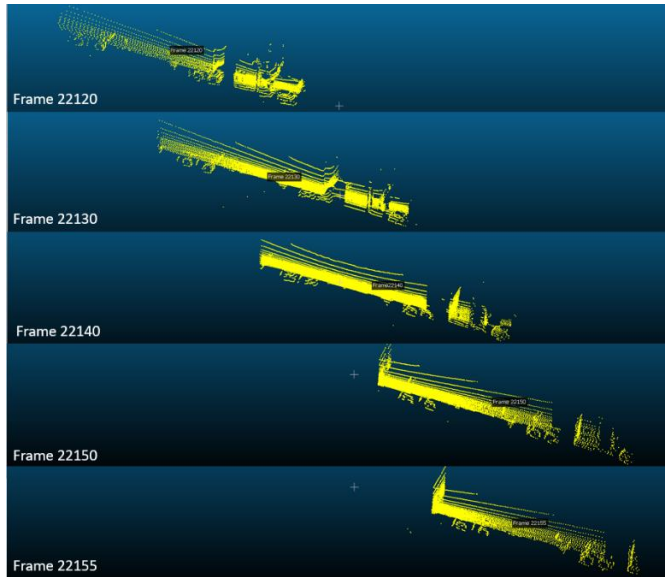


19

20 Figure 9 Samples of Redundant Frames

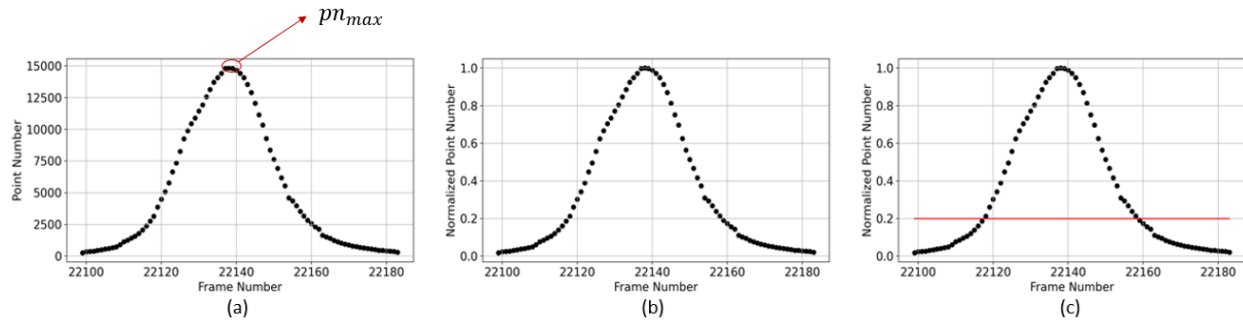
21 The sparse point cloud which is captured from these leading and trailing frames has a limited contribution  
22 to the registration process as the limited information details embedded in them are also captured in frames

1 captured when the truck is closer to the sensor (Figure 10). Hence, they can be eliminated to improve  
 2 computational efficiency.



3  
 4 Figure 10 Samples of Frames used for Registration

5 Figure 11a presents the point counts profile for a truck, which represents the total number of points captured  
 6 by the LiDAR in each frame while the truck traversed the LDZ. Frame 22,138 and Frame 22,139 contains  
 7 the highest number of points across all frames during its travel in the LDZ where the highest point count is  
 8 denoted as  $pn_{max}$  (Figure 11a). The point count profile is subsequently normalized based on  $pn_{max}$   
 9 (Figure 11b). Finally, the truck point cloud which contains point counts less than 20 percent of  $pn_{max}$   
 10 were treated as redundant frames and eliminated (Figure 11c).



11  
 12 Figure 11 Elimination of Redundant Frames

13  
 14 3.2.2 Statistical Outlier Removal and Voxel Down Sampling

15 After the background subtraction step, there still existed noises and outliers which were statistically  
 16 detectable. Therefore, an outlier removal process is needed prior to the vehicle point cloud registration.  
 17 This step involves two procedures: statistical outlier removal and voxel downsampling, which are suggested  
 18 by a popular 3D data processing library – Open3D (38). The statistical outlier removal method takes the 50  
 19 nearest neighbors of a given point in the point cloud and considers the points which are 2 standard deviations  
 20 in proximity from the given point as statistical outliers. Next, point clouds are further uniformly

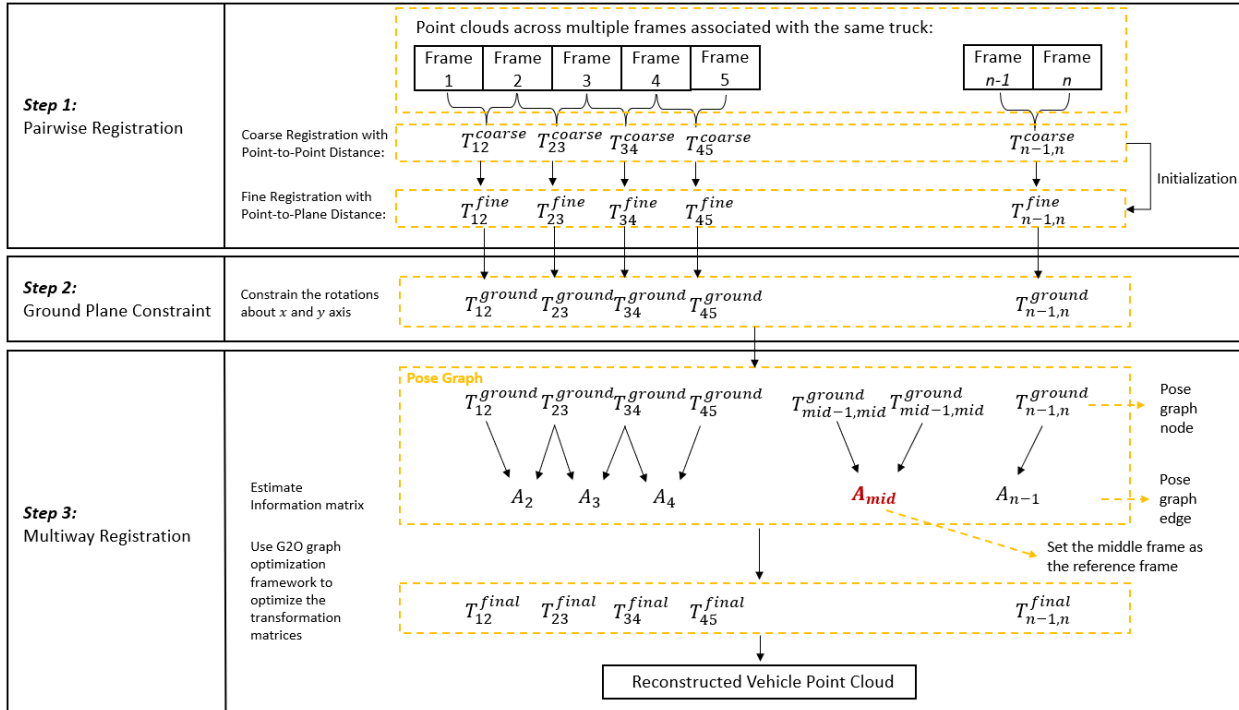
1 downsampling in order to increase the computational efficiency as well as preserve the structure of point  
 2 clouds, using a voxel downsampling approach where points are bucketed into voxel with the size of  $vs\_pre$   
 3 = 0.01 meter and represented by a single point which calculated through averaging all points within the  
 4 voxel.

### 5 3.2.3 Vehicle Point-Sets Registration

6 After the redundant frames and statistical outliers were removed, a pairwise registration with a coarse-to-  
 7 fine strategy was applied on each pair of adjacent frames. The pairwise alignment was accomplished  
 8 through the use of the FilterReg method (23). First, a coarse registration was conducted, where all point  
 9 clouds were coarsely downsampled with relatively larger voxel size  $vs\_coarse = 1.5$  meters, and each pair  
 10 of point clouds was subsequently aligned based on the point-to-point distances metric. Transformation  
 11 matrices were saved and denoted as  $\mathbf{T}_{j-1,j}^{coarse} = [T_{12}^{coarse}, T_{23}^{coarse}, T_{34}^{coarse}, \dots, T_{n-1,n}^{coarse}]$ , where  $j$  is the frame  
 12 index. Second, the  $\mathbf{T}_{j-1,j}^{coarse}$  was fine-tuned using point-to-plane distances with voxel size  $vs\_fine = 0.015$   
 13 meter. The transformation matrices obtained from fine registration was written as  $\mathbf{T}_{j-1,j}^{fine} =$   
 14  $[T_{12}^{fine}, T_{23}^{fine}, T_{34}^{fine}, \dots, T_{n-1,n}^{fine}]$ . Since the basic assumption about vehicle point clouds was that all the  
 15 point clouds associated with the same vehicle should land on the ground plane, the vehicles will not rotate  
 16 along the  $x$  and  $y$ -axis. Hence, the transformation matrices were constrained on  $x$ - and  $y$ -axis rotation, where  
 17 the corresponding elements in the matrices were set to zero, as shown in Equation 6:

$$18 \quad \mathbf{T}_{j-1,j}^{ground} = \begin{bmatrix} \cos\theta_z & -\sin\theta_z & 0 & t_x \\ \sin\theta_z & \cos\theta_z & 0 & t_y \\ 0 & 0 & 1 & t_z \\ 0 & 0 & 0 & 1 \end{bmatrix} \quad (6)$$

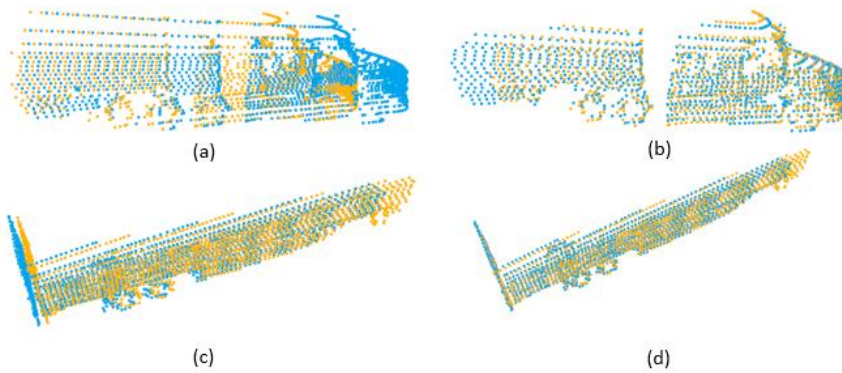
19 Third, in order to reduce the cumulative errors which could be potentially caused by sequential pairwise  
 20 registration, the transformation matrices were further optimized using the multiway registration which  
 21 described a process of merging multiple frames of an object in a global space. In this study, multiway  
 22 registration was implemented through the use of a pose graph optimization technique proposed in (24). The  
 23 multiway registration process is illustrated as follows. First, the information matrices which represent the  
 24 inversed correlation matrix between two consecutive transformation matrices were estimated. Second, a  
 25 pose graph is defined with the transformation matrices ( $\mathbf{T}_{j-1,j}^{ground}$ ) as the node and information matrices  
 26 ( $A_{n-1}$ ) as the edges in the graph, where each edge of the pose graph connects two nodes. The middle frame  
 27 of the vehicle object was set to be the reference frame with index  $j = mid = \text{ceil}(\frac{n}{2}, 0.5)$ . All frames were  
 28 aligned to the reference frame during the optimization process. The pose graph is optimized using the G2O  
 29 graph optimization framework (24). The final transformation matrices that were used to reconstruct the  
 30 vehicle point cloud were  $\mathbf{T}_{j-1,j}^{final} = [T_{12}^{final}, T_{23}^{final}, T_{34}^{final}, \dots, T_{n-1,n}^{final}]$ . The overall vehicle point cloud  
 31 registration framework is shown in Figure 12.



1

2 Figure 12 Vehicle Point Cloud Registration Framework

3 As a vehicle is approaching the LiDAR sensor, most of the information is captured from the very front of  
 4 the vehicle. The distinctive details as well as the level of the sparseness of the point cloud on the vehicle  
 5 make the process of finding corresponding points between two point clouds easier. Hence, minimizing the  
 6 point-to-point distance is capable of aligning the source (Yellow in Figure 13) to the target point cloud  
 7 (Blue in Figure 13) firmly. Figure 13a presents the point clouds of an individual vehicle traversing the LDZ  
 8 captured from two consecutive frames. Figure 13b shows the result of coarse registration with point-to-  
 9 point distance.



10

11 Figure 13 Examples of Pairwise Registration (Blue: target point cloud, Yellow: Source point cloud)

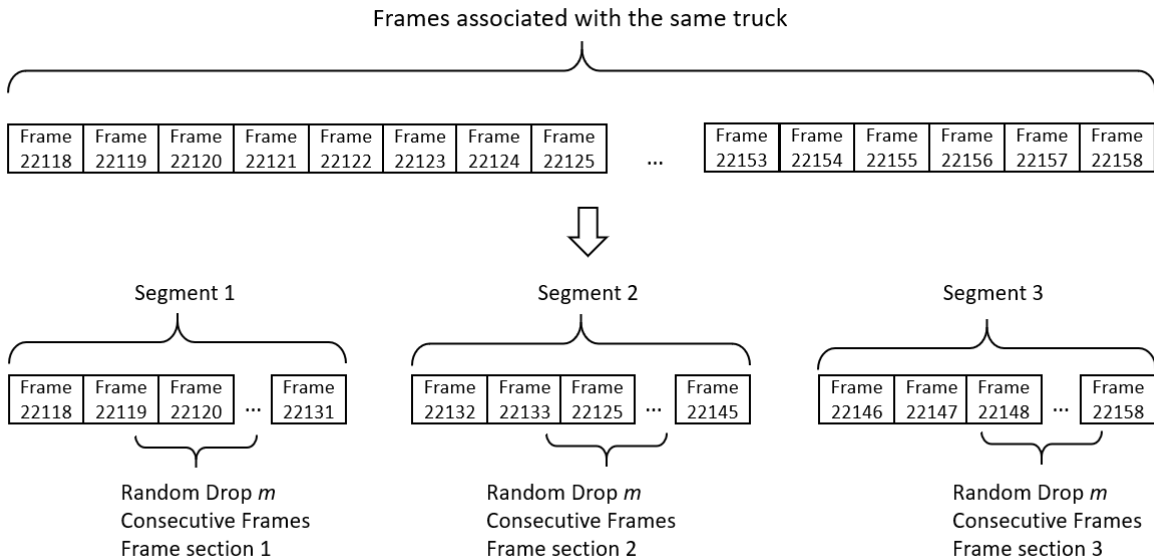
12 When the truck just passes the LiDAR sensor, captured points are densely distributed on the side of the  
 13 truck. However, the dimensional uniformity of some trailers such as enclosed vans and intermodal  
 14 containers results in only a limited number of prominent features captured even amongst the dense points.  
 15 This presents a challenge in achieving accurate alignments by solely minimizing the point-to-point distance.  
 16 Figure 13c shows a case in point where adjacent point cloud frames remain misaligned after coarse

1 registration using the point-to-point distance. However, the dense point distribution on the surface of the  
 2 truck’s side profile creates well-defined planes which allow the fine registration with the point-to-plane  
 3 strategy to successfully better align the two point clouds (Figure 13d).

4

### 5 3.2.4 Registration Performance with Missing Frames

6 The data used in this study was collected from a single-lane off-ramp section. Therefore, instances of  
 7 occluded vehicle point clouds were rarely observed in this data collection site. In order to test the robustness  
 8 of the new registration framework, random frames for a truck object were dropped to simulate missing  
 9 frames that may be caused by vehicle occlusions. Figure 14 demonstrates the experiment of the missing  
 10 frame test.



11

12

13 Figure 14 Illustration of Experiment Design

14 The duration of each vehicle traversing the LDZ was divided into three equal temporal segments denoted  
 15 by Segments 1 thru 3. Since vehicle occlusions typically occur across consecutive frames.  $m$  random  
 16 consecutive frames were dropped from each section at each time.

17 Figure 15 presents the results of the experiment. When 5 consecutive frames were dropped – equivalent to  
 18 0.5 seconds of missing data – from either Section 1 or Section 2, the reconstructed point cloud was still able  
 19 to preserve the essential information that could be used to identify their FHWA classes. For Section 3, the  
 20 reconstruction framework failed when the consecutive frame number equals 4. The random 5 consecutive  
 21 frames dropped from Segment 3 were the last 5 frames that are used for the vehicle reconstruction.  
 22 Therefore, nearly a quarter of the points on the rear truck wheel were missing.

23 This experiment demonstrated that the proposed framework is capable of reconstructing vehicle objects  
 24 with 3-5 consecutive missing frames. A comprehensive vehicle occlusion analysis will be further explored  
 25 after more real-world occlusion data are collected.

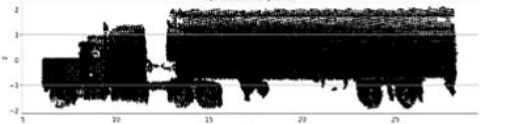

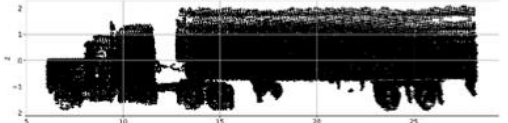
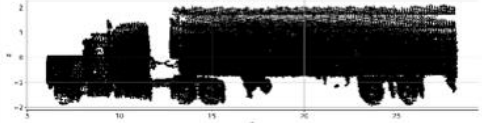

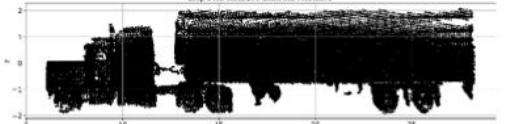
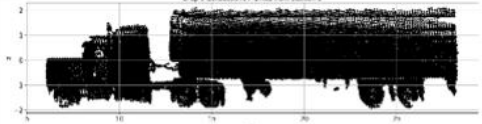

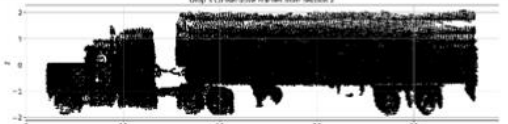
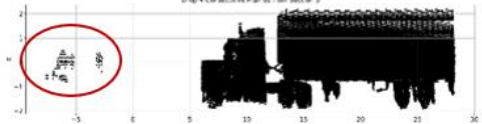



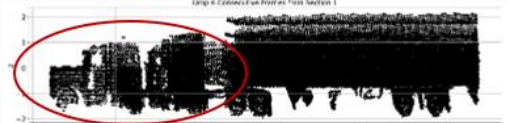

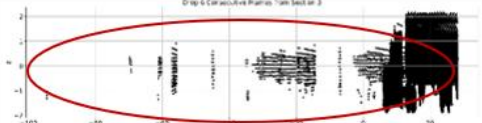
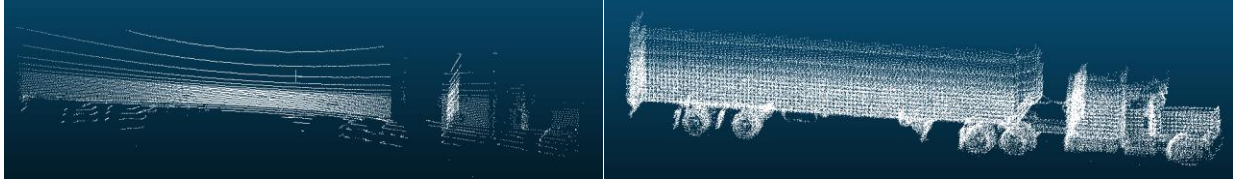
Number of Consecutive Frames	Segment 1: Approaching the LiDAR Sensor	Segment 2: In front of the LiDAR Sensor	Segment 3: Leaving the LiDAR Sensor
Drop 0 Frames	 <p style="text-align: center;">Original LiDAR Point Cloud</p>		
Random Drop 2 Consecutive Frames	 <p style="text-align: center;">Drop 2 Consecutive Frames from Section 1</p>	 <p style="text-align: center;">Drop 2 Consecutive Frames from Section 2</p>	 <p style="text-align: center;">Drop 2 Consecutive Frames from Section 3</p>
Random Drop 3 Consecutive Frames	 <p style="text-align: center;">Drop 3 Consecutive Frames from Section 1</p>	 <p style="text-align: center;">Drop 3 Consecutive Frames from Section 2</p>	 <p style="text-align: center;">Drop 3 Consecutive Frames from Section 3</p>
Random Drop 4 Consecutive Frames	 <p style="text-align: center;">Drop 4 Consecutive Frames from Section 1</p>	 <p style="text-align: center;">Drop 4 Consecutive Frames from Section 2</p>	 <p style="text-align: center;">Drop 4 Consecutive Frames from Section 3</p>
Random Drop 5 Consecutive Frames	 <p style="text-align: center;">Drop 5 Consecutive Frames from Section 1</p>	 <p style="text-align: center;">Drop 5 Consecutive Frames from Section 2</p>	 <p style="text-align: center;">Drop 5 Consecutive Frames from Section 3</p>
Random Drop 6 Consecutive Frames	 <p style="text-align: center;">Drop 6 Consecutive Frames from Section 1</p>	 <p style="text-align: center;">Drop 6 Consecutive Frames from Section 2</p>	 <p style="text-align: center;">Drop 6 Consecutive Frames from Section 3</p>
Random Drop 7 Consecutive Frames	Completely miss aligned	Completely miss aligned	Completely miss aligned

Figure 15 Experiment Results



#### 1 4. Ensemble Deep Neural Network for Axle-based Classification

2 The lower profile of a truck contains information related to its axle and general body configuration which  
3 defines their FHWA-CA classes. Compared to a single frame of a truck object, the lower profile of the  
4 reconstructed truck point cloud is well-defined (Figure 16).

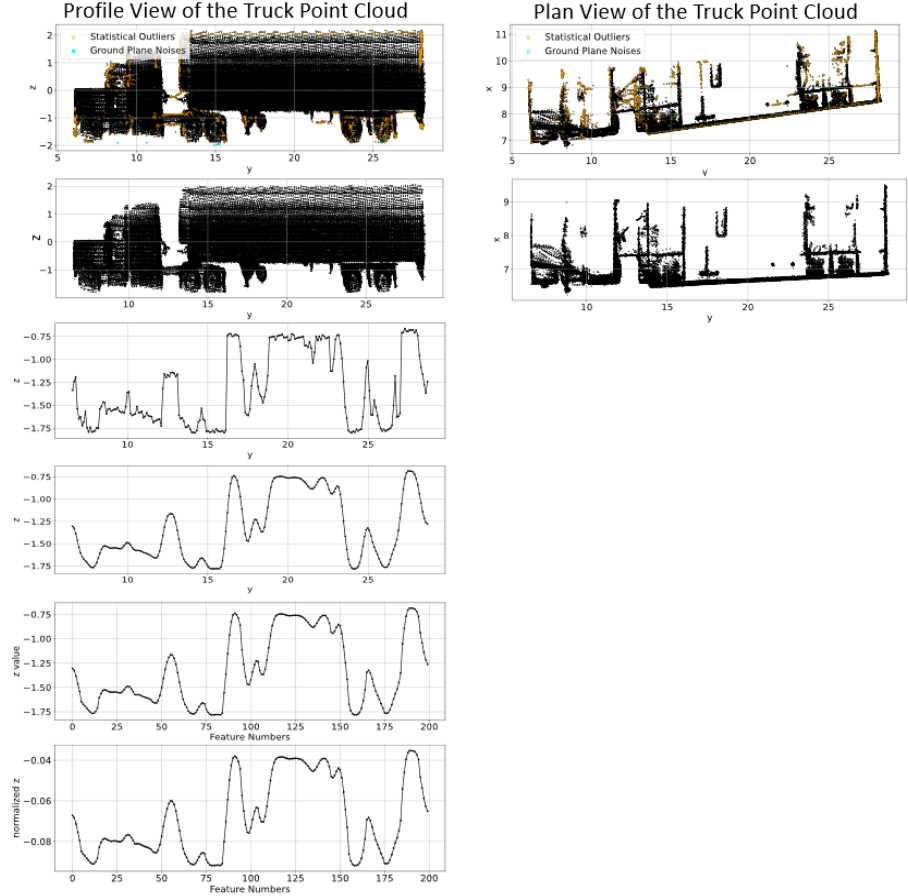
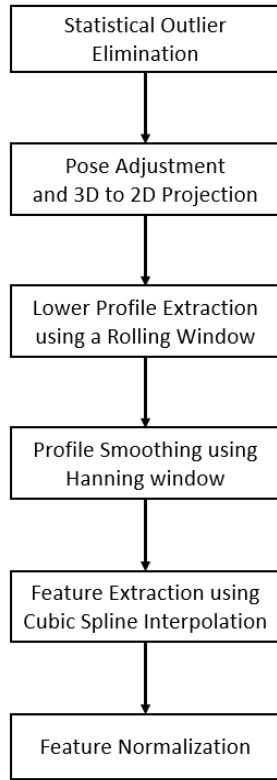


5  
6 Figure 16 Truck Object from a Single Frame (Left) vs. A Reconstructed Truck Point Cloud (Right)

7 Therefore, in this section, essential features from the lower profile of the reconstructed truck point cloud  
8 were extracted and used as inputs for the vehicle classification model. Next, a deep ensembled neural  
9 network model was developed to assign vehicle point clouds to their corresponding FHWA-CA classes.

##### 10 4.1 Feature Extraction

11 Prior to the feature extraction, statistical outliers on the reconstructed vehicle point cloud were further  
12 removed (38). Subsequently, the pose of the vehicle point cloud was adjusted to align with the zy plane  
13 using transformation matrix  $T_{mid-1,mid}$  since the middle frame was used as the reference frame in the pose  
14 graph optimization. Then, the 3D point cloud was projected to zy plane to obtain its 2D. The feature  
15 extraction process is shown Figure 17.



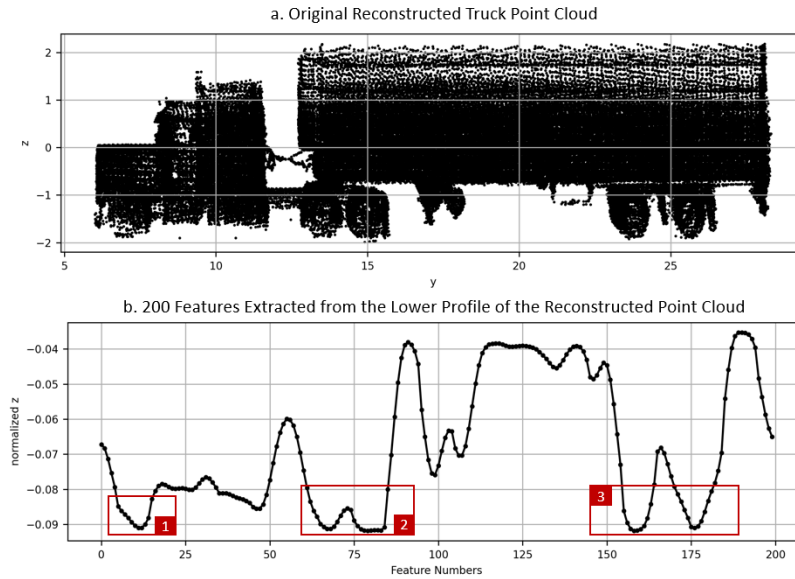
1  
2 Figure 17 Feature Extraction

3 First, a rolling window with a size of 0.1 was created, where the minimum  $z$  value within the window was  
4 calculated. The size of the rolling window should be less than the radius of a regular wheel of a truck. The  
5 minimum  $z$  value rolling window captures the raw lower profile of each vehicle point cloud. Second, in  
6 order to obtain a better representation of the lower profile, the raw profile was smoothed using Hann  
7 window (39) which is formulated as:

8 
$$w(i) = 0.5 - 0.5 \cos\left(\frac{2\pi i}{M-1}\right) \quad 0 \leq i \leq M-1, \quad (7)$$

9 where  $i$  represents the index of each point in the profile.  $M$  is the window size of the filter.

10 The smoothed lower profile of the truck point cloud presents both the axle and general body configuration  
11 of the truck. Third, the smoothed lower profiles were interpolated using cubic spline interpolation, and then  
12 200 equally spaced  $z$  values were extracted from the interpolated profile to align with the dimension of the  
13 training instances. Finally, the interpolated profile was normalized along the  $z$ -axis to the scale of -1 to 1.



1

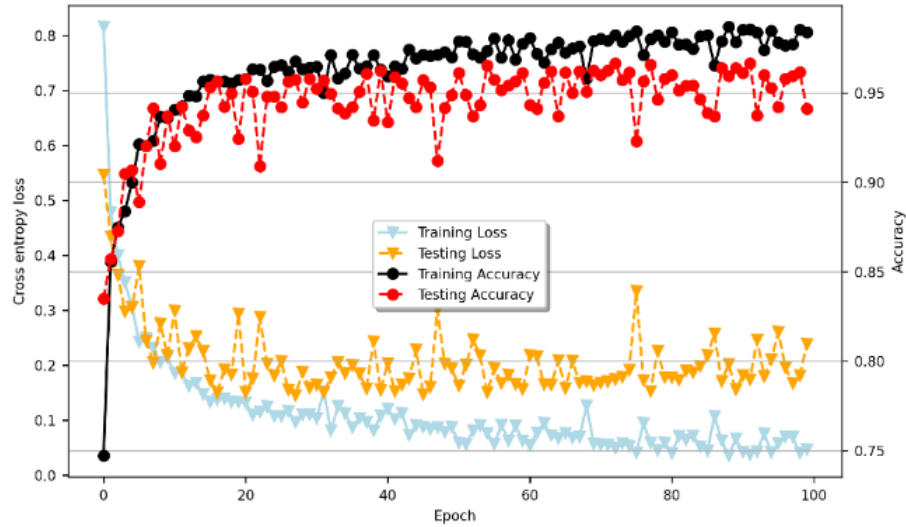
2 Figure 18 Illustration of Features

3 As Figure 18 shows, the valley in box 1 indicates the steering axle of the drive unit. Valleys in box 2  
 4 represent the drive axles of the drive unit and the valleys in box 3 capture the split axles on the trailer unit.

5

6 4.2 Bootstrap Aggregating (Bagging) Ensemble Deep Neural Network for Vehicle Classification

7 Neural Network models have been proved to be able to approximate any complex non-linear mapping  
 8 functions (40). Compare to the shallow neural network, a multi-layer structure of a deep neural network  
 9 model allows it to accomplish the same task with exponentially lower computation complexity (41).  
 10 Therefore, this study developed a deep neural network (DNN) with dropout regularization (42) to assign  
 11 each vehicle point cloud to its corresponding FHWA-CA classes. The DNN model comprised 5 hidden  
 12 layers with 512 neurons on each layer. Thirty percent of neurons were randomly dropped out on the last  
 13 two hidden layers to remedy the overfitting issue. The Rectified Linear Unit (ReLU) (43) with He  
 14 initialization method (44) was applied to each hidden layer and the Softmax activation function with Xavier  
 15 initialization (45) was used on the output layer. The learning curve shown in Figure 19 traces the model  
 16 performance histories during the training and testing process. After 100 epochs, the overall accuracy on the  
 17 training set keeps gradually increasing while the testing accuracy converge to 0.95. Hence the model  
 18 training converged after 100 epochs.



1  
2 Figure 19 Learning Curve

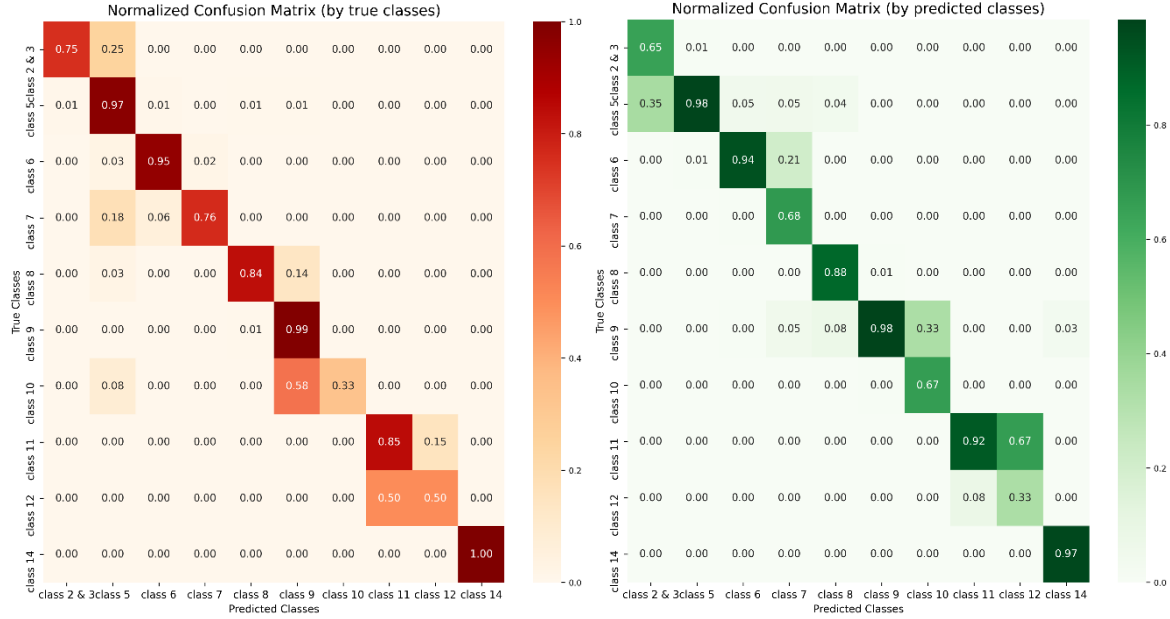
3 In order to reduce the variability of the DNN prediction results, a bootstrap aggregating (bagging) (46)  
4 ensemble approach was applied. Using stratified bootstrap resampling strategy (47), the bagging ensemble  
5 method resampled the training set to ten sets of bootstrapped training samples which were used to build ten  
6 different DNN models with the same model structure. The final prediction results are determined by the  
7 highest averaged prediction score of the ten DNN models.

8  
9 **5. Model Results**

10 This section presents the testing results of the model developed in this study using a normalized confusion  
11 matrix and then provides the error analysis on the misclassified vehicles. In addition, the developed model  
12 was compared with the state-of-the-art FHWA axle-based classification model using a LiDAR sensor.

13 **5.1 Classification Results and Analysis**

14 The normalized confusion matrix of the classification model is presented in Figure 20.



1  
2 Figure 20 Normalized Confusion Matrix for the Test Set

3 Each row of the red-colored confusion matrix is normalized by the total number of groundtruth vehicle  
4 counts in their corresponding classes. Therefore, the diagonal elements represent the recall values of each  
5 class, which was also referred to as “Correct Classification Rate” (CCR) in some literature (21, 48). The  
6 recall value is calculated as follow:

$$7 \quad Recall = \frac{TP}{TP + FN}, \quad (8)$$

8 where  $TP$  denotes true positives and  $FN$  is the true negatives.

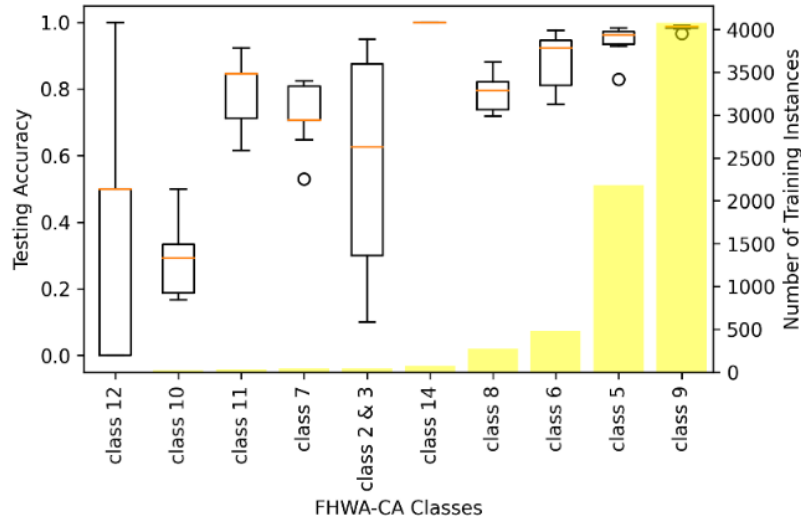
9 Each column of the green-colored confusion matrix is normalized according to the total number of predicted  
10 values for each class. Hence, the diagonal elements are the precision values of each class.

$$11 \quad Precision = \frac{TP}{TP + FP}, \quad (9)$$

12 where  $FP$  represents the false positives.

13 Based on the normalized confusion matrices, the proposed model was able to correctly classify Classes 5,  
14 6, 8, 11, and 14 with over 80 percent CCR. However, the model did not perform as well in predicting  
15 Classes 10 and 12. Notwithstanding, in terms of Class 10, the precision value is higher than the recall value  
16 which means when this model is implemented, very few predictions on Class 10 will be received within  
17 which most of them will be correctly classified. Conversely, Class 12 has a higher recall than its precision  
18 value which would cause that the model to return higher than actual counts of Class 12 predictions, with  
19 most of them being misclassifications from other classes.

20 The boxplot in Figure 21 shows the model recall distribution of the DNN models which are built with 10  
21 sets of bootstrapped training instances. The bar plot represents the training sample size for each class.

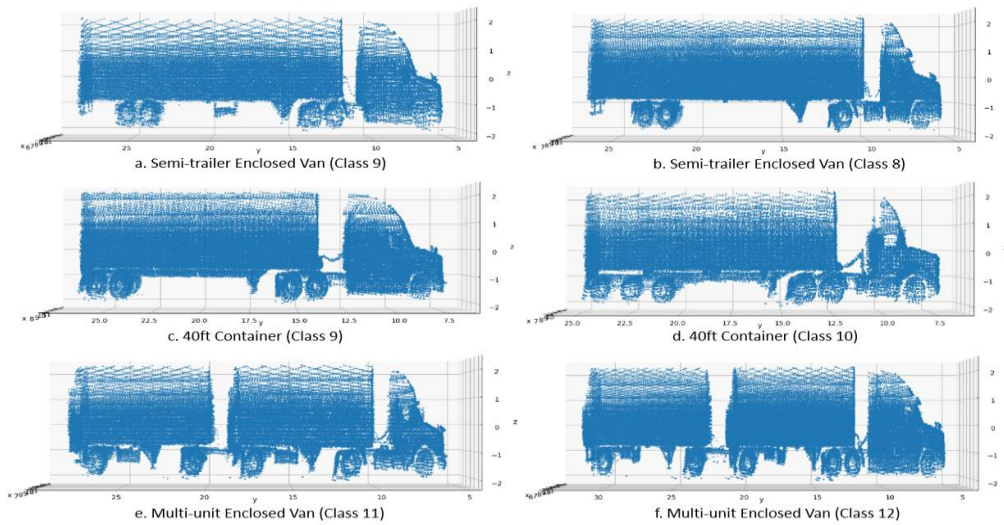


1

2 Figure 21 CCR and Train Counts Distribution across classes

3 As Figure 21 shows, the model performance on the classes with lower instances training samples tends to have higher  
 4 variability in the prediction results, especially for Classes 2&3, and 12. Insufficient training samples were  
 5 used to learn the key features from Classes 10 and 12 trucks which resulted in high variances in their  
 6 prediction outcomes. In addition, Classes 2 and 3, passenger vehicles, were rarely observed at the entrance  
 7 of the truck scale and those vehicles have larger diversity in terms of their body shape. Therefore, the model  
 8 prediction variance is also high for Classes 2 and 3. Even though there is a limited number of training  
 9 samples for Class 14, its prediction results are still promising since Class 14 represents a small  
 10 homogeneous subpopulation of trucks.

11 With sufficient training samples, the proposed classification model is capable of accurately distinguishing  
 12 Classes 8 and 9 with overlapping body configuration (Figure 22a and b). However, Classes which have  
 13 minor differences in their axle configuration but with the same body type are hard to distinguish when the  
 14 sample size is small (Figure 22c, d, e, and f). Consequently, the training dataset needs to be enriched in  
 15 future studies to further enhance the model performance on Classes 10 and 12.



16

17 Figure 22 Overlapping Body Configurations

1 5.2 Model Comparison

2 The proposed model has been compared with the state-of-the-art LiDAR-based classification model which  
 3 used the single frame of an object to classify vehicles on the basis of the FHWA scheme (22). The model  
 4 comparison is shown in Table 1.

5 Table 1 Model Comparison

FHWA-CA	CCR (Bagging DNN)	Testing Samples	Classes defined in (22)	CCR (Random Forest) (22)	Testing Samples (22)
Class 2	0.75	20	Passenger Vehicle	0.84	150
Class 3			Four-tire Single Unit	0.70	69
Class 4	None	None	Bus	1.00	20
Class 5 <sup>1</sup>	0.97	934	Two-axle, six-tire, single-unit truck	0.44	17
Class 6	0.95	208	Three-axle, single-unit truck	0.00	4
Class 7	0.76	17	Four or fewer axle, single-trailer truck	None	None
Class 8	0.84	117	None	None	None
Class 9 <sup>2</sup>	0.99	1,746	Five-axle, single-trailer truck	1.00	17
Class 10	0.33	12	None	None	None
Class 11	0.85	13	None	None	None
Class 12	0.50	2	None	None	None
Class 13	None	None	None	None	None
Class 14	1.00	31	None	None	None
Average CCR	0.79	-	-	0.76	-

6 Note: <sup>1</sup>Class 5 used in this study contained the two-axle truck pulling a small trailer which was not included in (22). <sup>2</sup>In the FHWA-CA scheme,  
 7 Class 9 type 32 was separated from the rest of Class 9 truck and labeled as Class 14. In (22), Class 14 trucks are merged into Class 9 trucks.

8 Compared to the previous model (22), the new classification framework proposed in this study is able to  
 9 classify the vehicle in much more detail with significantly higher accuracy, especially for heavy-duty truck  
 10 categories from Class 8 to Class 14, where they have disproportionately adverse impacts on the pavement  
 11 (1) and the environment (2).

12

13 **6. Conclusions and Future Work**

14 This research designed a novel vehicle point cloud reconstruction framework with the ground plane  
 15 constraint that registers consecutive frames associated with the same vehicle to enrich the sparse point cloud  
 16 from each scan of the LiDAR sensor. This vehicle point cloud reconstruction framework adopts a horizontal  
 17 orientation of the LiDAR sensor which provides a panoramic view of the roadway environment without  
 18 compromising the robustness of the classification framework. Furthermore, an ad-hoc testing was applied  
 19 to the vehicle reconstruction framework to examine its robustness under the simulation of dropped frames  
 20 caused by occlusion. The reconstruction framework was capable of handling 3-5 consecutive missing  
 21 frames and demonstrating the significant potential for multi-lane applications. The axle, as well as body  
 22 configuration of the reconstructed vehicle point clouds, are well-defined. Critical features which are used  
 23 to describe FHWA-CA classes were extracted from the lower profile of the reconstructed point clouds. A  
 24 bagging DNN model was developed to classify the lower profile of the reconstructed vehicle point cloud  
 25 based on the FHWA-CA scheme. The proposed classification framework yields accurate prediction results,  
 26 especially on heavy-duty trucks such as Classes 8, 9, 11, and 14 with CCR of 0.84, 0.99, 0.85, 1.00,  
 27 respectively. According to the result analysis, the proposed model is also capable of distinguishing Classes  
 28 3, 5, and 8 which have overlapping axle configurations and are often misclassified by WIM systems (7).  
 29 The proposed model also performed very well in distinguishing Classes 8 and 9 which have overlapping

1 body configurations, with limited success obtained by inductive signature models (12). In addition, the  
2 proposed classification framework was able to obtain an average CCR of 79 percent on the test dataset and  
3 outperforms the state-of-the-art LiDAR-based FHWA vehicle classification model in terms of both  
4 accuracy and robustness.

5 In the future, this framework will be tested on other spatially independent sites. Its ability for multi-lane  
6 applications will also be examined with real-world data.

7

8 **Acknowledgment**

9 This study was made possible through funding received by the California Department of Transportation  
10 (Caltrans) and the Pacific Southwest Region University Transportation Center (PSR-UTC). The authors  
11 would like to thank Caltrans and PSR-UTC for their support of university-based research, and especially  
12 for the funding received for this project. The authors also gratefully appreciate the assistance provided by  
13 Tom Shepard of Caltrans District 11 for his innovative efforts in installing the field sensors. The contents  
14 of this paper reflect the views of the authors who are responsible for the facts and the accuracy of the data  
15 presented herein. The contents do not necessarily reflect the official views or policies of the State of  
16 California. This paper does not constitute a standard, specification, or regulation.

17

18

19 **Author Contributions**

20 The authors confirm contribution to the paper as follows: study conception and design: Yiqiao Li, Andre  
21 Tok, Stephen G. Ritchie; data collection: Yiqiao Li, Andre Tok, Zhe Sun, Koti Reddy Allu; analysis and  
22 interpretation of results: Yiqiao Li, Andre Tok; draft manuscript preparation: Yiqiao Li, Andre Tok, Zhe  
23 Sun, Stephen G. Ritchie. All authors reviewed the results and approved the final version of the manuscript.

24



1 **Reference:**

- 2 1. Gillespie, T. D., Karamihas, S. M., & Sayer, M. W. *Effects of Heavy-Vehicle Characteristics on*  
3 *Paveemnt Response and Performance (NCHRP Report 353)*. 1993.
- 4 2. Guensler, R., S. Yoon, H. Li, and J. Jun. *Heavy-Duty Diesel Vehicle Modal Emission Model*  
5 *(HDDV-MEM) Volume I: Modal Emission Modeling Framework*. 2005.
- 6 3. Schaefer, Ron; Worth, Monica; Heilman, Jonathan; Kehoe, N. *Freight Demand Modeling and*  
7 *Data Improvement*. 2017.
- 8 4. Beagan, D., D. Tempesta, and K. Proussaloglou. *Quick Response Freight Methods (QRFM)*. 2019.
- 9 5. Federal Highway Administration. *Traffic Monitoring Guide FHWA*. 2013.
- 10 6. Kwigizile, V., R. N. Mussa, and M. Selekwa. Connectionist Approach to Improving Highway  
11 Vehicle Classification Schemes - The Florida Case. *Journal of the Transportation Research*  
12 *Board*, No. 1917, 2005, pp. 182–189.
- 13 7. Bitar, N., and H. H. Refai. A Probabilistic Approach to Improve the Accuracy of Axle-Based  
14 Automatic Vehicle Classifiers. *IEEE Transactions on Intelligent Transportation Systems*, Vol. 18,  
15 No. 3, 2017, pp. 537–544. <https://doi.org/10.1109/TITS.2016.2580058>.
- 16 8. Zhang, W., Q. Wang, and C. Suo. A Novel Vehicle Classification Using Embedded Strain Gauge  
17 Sensors. *Sensors*, Vol. 8, No. 11, 2008, pp. 6952–6971. <https://doi.org/10.3390/s8116952>.
- 18 9. Bajwa, R., R. Rajagopal, P. Varaiya, and R. Kavalier. In-Pavement Wireless Sensor Network for  
19 Vehicle Classification. *Proceedings of the 10th ACM/IEEE International Conference on*  
20 *Information Processing in Sensor Networks, IPSN'11*, 2011, pp. 85–96.
- 21 10. Ma, W., D. Xing, A. McKee, R. Bajwa, C. Flores, B. Fuller, and P. Varaiya. A Wireless  
22 Accelerometer-Based Automatic Vehicle Classification Prototype System. *IEEE Transactions on*  
23 *Intelligent Transportation Systems*, Vol. 15, No. 1, 2014, pp. 104–111.  
24 <https://doi.org/10.1109/TITS.2013.2273488>.
- 25 11. Jeng, S. T., and S. G. Ritchie. Real-Time Vehicle Classification Using Inductive Loop Signature  
26 Data. *Transportation Research Record*, No. 2086, 2008, pp. 8–22. [https://doi.org/10.3141/2086-](https://doi.org/10.3141/2086-02)  
27 [02](https://doi.org/10.3141/2086-02).
- 28 12. Jeng, S. T., L. Chu, and S. Hernandez. Wavelet-k Nearest Neighbor Vehicle Classification  
29 Approach with Inductive Loop Signatures. *Transportation Research Record*, No. 2380, 2013, pp.  
30 72–80. <https://doi.org/10.3141/2380-08>.
- 31 13. Wei, H., H. Abrishami, X. Xiao, and A. Karteek. Adaptive Video-Based Vehicle Classification  
32 Technique for Monitoring Traffic Prepared By : No. 134874, 2015.
- 33 14. Abdelbaki, H. M., K. Hussain, and E. Gelenbe. A Laser Intensity Image-Based Automatic Vehicle  
34 Classification System. *IEEE Conference on Intelligent Transportation Systems, Proceedings,*  
35 *ITSC*, 2001, pp. 460–465. <https://doi.org/10.1109/itsc.2001.948701>.
- 36 15. Hussain, K. F., and G. S. Moussa. Laser Intensity Vehicle Classification System Based on  
37 Random Neural Network. *Proceedings of the Annual Southeast Conference*, Vol. 1, 2005, pp.  
38 131–135. <https://doi.org/10.1145/1167350.1167372>.
- 39 16. Sandhawaliala, H., J. A. Rodriguez-Serrano, H. Poirier, and G. Csurka. Vehicle Type Classification  
40 from Laser Scanner Profiles: A Benchmark of Feature Descriptors. *IEEE Conference on*  
41 *Intelligent Transportation Systems, Proceedings, ITSC*, No. Itsc, 2013, pp. 517–522.

- 1 <https://doi.org/10.1109/ITSC.2013.6728283>.
- 2 17. Lee, H., and B. Coifman. Side-Fire Lidar-Based Vehicle Classification. *Transportation Research*  
3 *Record*, No. 2308, 2012, pp. 173–183. <https://doi.org/10.3141/2308-19>.
- 4 18. Asborn, M. I., C. G. Burris, and S. Hernandez. Truck Body-Type Classification Using Single-  
5 Beam Lidar Sensors. *Transportation Research Record*, Vol. 2673, No. 1, 2019, pp. 26–40.  
6 <https://doi.org/10.1177/0361198118821847>.
- 7 19. Vatani Nezafat, R., O. Sahin, and M. Cetin. Transfer Learning Using Deep Neural Networks for  
8 Classification of Truck Body Types Based on Side-Fire Lidar Data. *Journal of Big Data Analytics*  
9 *in Transportation*, Vol. 1, No. 1, 2019, pp. 71–82. <https://doi.org/10.1007/s42421-019-00005-9>.
- 10 20. Velodyne Acoustics Inc. *VLP-32C User Manual*. 2018.
- 11 21. Sahin, O., R. V. Nezafat, and M. Cetin. Methods for Classification of Truck Trailers Using Side-  
12 Fire Light Detection and Ranging (LiDAR) Data. *Journal of Intelligent Transportation Systems:*  
13 *Technology, Planning, and Operations*, Vol. 0, No. 0, 2020, pp. 1–13.  
14 <https://doi.org/10.1080/15472450.2020.1733999>.
- 15 22. Wu, J., H. Xu, Y. Zheng, Y. Zhang, B. Lv, and Z. Tian. Automatic Vehicle Classification Using  
16 Roadside LiDAR Data. *Transportation Research Record*, Vol. 2673, No. 6, 2019, pp. 153–164.  
17 <https://doi.org/10.1177/0361198119843857>.
- 18 23. Gao, W., and R. Tedrake. Filterreg: Robust and Efficient Probabilistic Point-Set Registration  
19 Using Gaussian Filter and Twist Parameterization. *Proceedings of the IEEE Computer Society*  
20 *Conference on Computer Vision and Pattern Recognition*, Vol. 2019-June, 2019, pp. 11087–  
21 11096. <https://doi.org/10.1109/CVPR.2019.01135>.
- 22 24. Choi, S., Q. Y. Zhou, and V. Koltun. Robust Reconstruction of Indoor Scenes. *Proceedings of the*  
23 *IEEE Computer Society Conference on Computer Vision and Pattern Recognition*, Vol. 07-12-  
24 June, 2015, pp. 5556–5565. <https://doi.org/10.1109/CVPR.2015.7299195>.
- 25 25. Li, Y., K. Allu, Z. Sun, A. Tok, G. Feng, and S. Ritchie. An Ensemble Approach to Truck Body  
26 Type Classification Using Deep Representation Learning on 3D Point Sets. 2021.
- 27 26. Daszykowski, M., and B. Walczak. A Density-Based Algorithm for Discovering Clusters in Large  
28 Spatial Databases with Noise. *Kdd*, Vol. 96, 1996, pp. 226–231. <https://doi.org/10.1016/B978-044452701-1.00067-3>.
- 30 27. Bewley, A., Z. Ge, L. Ott, F. Ramos, and B. Uppcroft. Simple Online and Realtime Tracking.  
31 *Proceedings - International Conference on Image Processing, ICIP*, Vol. 2016-Augus, 2016, pp.  
32 3464–3468. <https://doi.org/10.1109/ICIP.2016.7533003>.
- 33 28. Kalman, R. E. A New Approach to Linear Filtering and Prediction Problems. *Journal of Fluids*  
34 *Engineering, Transactions of the ASME*, Vol. 82, No. 1, 1960, pp. 35–45.  
35 <https://doi.org/10.1115/1.3662552>.
- 36 29. Kuhn, H. W. The Hungarian Method for the Assignment Problem. *Naval Research Logistics*, Vol.  
37 2, No. 1–2, 1955, pp. 83–97. <https://doi.org/10.1002/nav.20053>.
- 38 30. Besl, P., and N. McKay. A Method for Registration of 3D Shapes. *IEEE Transactions on Pattern*  
39 *Analysis and Machine Intelligence*, Vol. 14, No. 2, 1992, pp. 239–256.
- 40 31. Chen, Y., and G. Medioni. Object Modeling by Registration of Multiple Range Images.  
41 *Proceedings - IEEE International Conference on Robotics and Automation*. 2724–2729.

- 1 <https://graphics.stanford.edu/~smr/ICP/comparison/chen-medioni-align-rob91.pdf>.
- 2 32. Pomerleau, F., F. Colas, and R. Siegwart. A Review of Point Cloud Registration Algorithms for  
3 Mobile Robotics. *A Review of Point Cloud Registration Algorithms for Mobile Robotics*, 2015.  
4 <https://doi.org/10.1561/9781680830255>.
- 5 33. Pomerleau, F., F. Colas, R. Siegwart, S. Magnenat, F. Pomerleau, F. Colas, R. Siegwart, S.  
6 Magnenat, C. Icp, and F. C. Roland. Comparing ICP Variants on Real-World Data Sets.  
7 *Autonomous Robots*, Vol. 34, No. 3, 2013, pp. 133–148.
- 8 34. Myronenko, A., and X. Song. Point Set Registration: Coherent Point Drifts. *IEEE Transactions on*  
9 *Pattern Analysis and Machine Intelligence*, Vol. 32, No. 12, 2010, pp. 2262–2275.  
10 <https://doi.org/10.1109/TPAMI.2010.46>.
- 11 35. Jian, B., I. C. Society, and B. C. Vemuri. Robust Point Set Registration Using Gaussian Mixture  
12 Models. *IEEE Transactions on Pattern Analysis and Machine Intelligence*, Vol. 33, No. 8, 2011,  
13 pp. 1633–1645.
- 14 36. Horaud, R., F. Forbes, M. Yguel, G. Dewaele, and J. Zhang. Rigid and Articulated Point  
15 Registration with Expectation Conditional Maximization. *IEEE Transactions on Pattern Analysis*  
16 *and Machine Intelligence*, Vol. 33, No. 3, 2011, pp. 587–602.  
17 <https://doi.org/10.1109/TPAMI.2010.94>.
- 18 37. Evangelidis, G. D., D. Kounades-Bastian, R. Horaud, and E. Z. Psarakis. A Generative Model for  
19 the Joint Registration of Multiple Point Sets. *Lecture Notes in Computer Science (including*  
20 *subseries Lecture Notes in Artificial Intelligence and Lecture Notes in Bioinformatics)*, Vol. 8695  
21 LNCS, No. PART 7, 2014, pp. 109–122. [https://doi.org/10.1007/978-3-319-10584-0\\_8](https://doi.org/10.1007/978-3-319-10584-0_8).
- 22 38. Zhou, Q. Y., J. Park, and V. Koltun. Open3D: A Modern Library for 3D Data Processing. *arXiv*,  
23 2018.
- 24 39. Oppenheim, V., A., R. Schafer, W., and J. Buck, R. *Discrete-Time Signal Processing*. Prentice-  
25 Hall, Inc., 1999.
- 26 40. Hornik, K., M. Stinchcombe, and H. White. Multilayer Feedforward Networks Are Universal  
27 Approximators. *Neural Networks*, Vol. 2, No. 5, 1989, pp. 359–366. [https://doi.org/10.1016/0893-](https://doi.org/10.1016/0893-6080(89)90020-8)  
28 [6080\(89\)90020-8](https://doi.org/10.1016/0893-6080(89)90020-8).
- 29 41. Shiyu Liang; R. Srikant. Why Deep Neural Networks for Function Approximation? 2017.
- 30 42. Mele, B., and G. Altarelli. Dropout: A Simple Way to Prevent Neural Networks from Overfitting.  
31 *Physics Letters B*, Vol. 299, No. 3–4, 2014, pp. 345–350. [https://doi.org/10.1016/0370-](https://doi.org/10.1016/0370-2693(93)90272-J)  
32 [2693\(93\)90272-J](https://doi.org/10.1016/0370-2693(93)90272-J).
- 33 43. Nair, V., and G. E. Hinton. Rectified Linear Units Improve Restricted Boltzmann Machines.  
34 *Proceedings of the 27th International Conference on Machine Learning*, No. 3, 2010, pp. 807–  
35 814. <https://doi.org/10.1.1.165.6419>.
- 36 44. He, K., X. Zhang, S. Ren, and J. Sun. Delving Deep into Rectifiers: Surpassing Human-Level  
37 Performance on Imagenet Classification. *Proceedings of the IEEE International Conference on*  
38 *Computer Vision*, Vol. 2015 Inter, 2015, pp. 1026–1034. <https://doi.org/10.1109/ICCV.2015.123>.
- 39 45. Glorot, X., and Y. Bengio. Understanding the Difficulty of Training Deep Feedforward Neural  
40 Networks. *Journal of Machine Learning Research*, Vol. 9, 2010, pp. 249–256.
- 41 46. Breiman, L. Bagging Predictors: Technical Report No. 421. *Department of Statistics University of*

1            *California*, No. 2, 1994, p. 19.

2    47.    Efron, B. Bootstrap Methods: Another Look at the Jackknife. *Annals of Statistics*, Vol. 2, No. 5,  
3            1988, pp. 347–370.

4    48.    Hernandez, S. V., A. Tok, and S. G. Ritchie. Integration of Weigh-in-Motion (WIM) and Inductive  
5            Signature Data for Truck Body Classification. *Transportation Research Part C: Emerging*  
6            *Technologies*, Vol. 68, 2016, pp. 1–21. <https://doi.org/10.1016/j.trc.2016.03.003>.

7

8